Thermal Analysis of Thermal Barrier Coatings in a High Heat Flux Environment

J.A. Nesbitt and W.J. Brindley
NASA Lewis Research Center
Cleveland, OH

INTRODUCTION

A gaseous H_2/O_2 rocket engine was constructed at NASA-Lewis Research Center (LeRC) to test the durability of thermal barrier coatings (TBC's) in a high heat flux environment. The purpose for this work was to evaluate the potential use of TBC's on the blades in the high-pressure fuel turbopump (HPFTP) on the space shuttle main engines (SSME). These blades undergo a thermal shock due to thermal transients which are present on startup and shutdown of the engine. This thermal shock is believed to contribute to the formation and/or propagation of cracks in the blades which results in their replacement significantly before the design life of the engine. Durability testing of TBC's in the rocket engine is discussed in a companion paper (Ref. 1).

The purpose of the present work was to evaluate the thermal environment within the rocket engine at LeRC and to perform a thermal analysis of the test specimens with and without TBC's. Test specimens consisted of 0.953 cm (0.375 in) O.D tubes and rods and were located at the throat of the rocket engine. Three different thermocouple probe designs were used to measure hot gas temperatures. One probe design permitted a thermal analysis of the probe itself to evaluate the corrections for recovery, conduction and radiation. The angular dependence of the pressure around the test specimen was also measured. Heat transfer coefficients were measured at two positions on the cylindrical surface by use of an instrumented, water-cooled stainless steel tube.

A thermal analysis of bare and coated tubes and rods was performed using the measured gas temperatures and heat transfer coefficients. Predicted metal temperatures were compared with measured temperatures on several instrumented tubes.

The beneficial effect of TBC's on decreasing peak metal temperatures in the HPFTP was examined by performing a thermal analysis at the leading edge of an HPFTP blade for the temperature spike which occurs on ignition of the SSME. The thermal analysis shows that TBC's have significant potential to reduce the thermal shock to the leading edge of the blades.

EXPERIMENTAL

A schematic of the rocket engine and the copper specimen holder is shown in Fig. 1. Five 0.953 cm (0.375 in) tubes or rods are held in the copper specimen holder which is positioned at the rear of the engine such that all gas flow is perpendicular to the cylindrical

axis. The hot gas from the combustion chamber is constricted by the presence of the tubes which form the throat of the rocket engine forcing the exhaust gas velocity to reach Mach 1 at the throat plane. Only three of the five specimens are fully exposed in the gas flow. All durability testing of TBC's was performed with specimens in test position 2 for reasons explained in Reference 1. Consequently, gas temperatures and pressures were only measured near this position.

Most gas temperature measurements were made at an oxidizer to fuel mass ratio (O/F) equal to 1 calculated from flow rates into the engine. This O/F ratio resulted in a hydrogen-rich environment far below stoichiometric compositions (O/F=7.94) The pressure in the chamber of the rocket engine was maintained at approximately 2.07 Mpa (300 psi) and generally varied from day to day by less than 3%. The predicted adiabatic gas temperature for this O/F ratio and pressure is 1000°C (1832°F). Standard operation of the engine involved a 0.1 second lead with O_2 before opening the H_2 valve. Generally the hot fire duration was 1.3 seconds but was extended up to 3.3 seconds for several tests. At the end of the hot fire, the closing of the H_2 valve was delayed 0.3 seconds following the closing of the O_2 valve which resulted in a short H_2 purge. As the O_2 and H_2 valves were closed, gaseous N_2 was passed through the injector to rapidly cool the specimens to room temperature.

Three thermocouple configurations were used to measure gas temperatures: butt-welded, shielded and wedge-type thermocouples (Fig. 2). All thermocouple assemblies consisted of either Type R or Type B wire running through alumina or magnesia sheathing which was slid into 0.318 cm (0.125 in) OD molybdenum (Mo) tubes. The shields on the shielded thermocouples were also fabricated from Mo and welded to the Mo tube. Wire diameters varied from 0.0254 to 0.0635 cm (0.010 to 0.025 in). Alumina or magnesia sheathing without the Mo tubes fractured during hot firings. The shielded thermocouples were located on the injector side of the throat plane at positions indicated A1 and A2. The butt-welded thermocouples were run at positions indicated B1 and B2 such that the gas flow was perpendicular to the wire axis. The wedge-type thermocouples were located behind the specimen at the position indicated C. Gas temperature measurements were made as close as possible to the midpoint of the throat opening. Most thermocouples survived only 1 or 2 hot firings because of the high temperatures, thermal shock and gas forces on the thermocouples.

Heat transfer coefficients (h_c) were measured with an instrumented stainless steel tube. A schematic cross section of the instrumented tube is shown in Figure 3. The 0.953 cm OD, 0.648 cm ID (0.375 in OD, 0.255 in ID) tube was initially cut into two halves. Channels 0.038 cm (0.015 in) in depth by 0.030 cm (0.012 in) width were cut on the inside and outside of the tube wall and 0.0254 cm (0.010 in) sheathed thermocouples were placed in the channels and the beads welded to the bottom of the channel. The channels were covered with a 0.013 cm (0.005 in) Inconel 600 sheet which was welded in place to seal the channel from the hot gasses. Large slots were also cut into the tube wall and filled with high-temperature ceramic cement to reduce

tangential heat flow within the tube wall. Identical channels were cut in both halves of the tube to allow wall temperatures to be measured at two locations 180° apart. The two halves were welded back together and the weld seam was smoothed to match the contour of the tube. The instrumented tube was placed in a special Cu specimen holder which permitted the tube to be water cooled. The difference in temperature across the wall, along with the measured gas temperature, allowed calculation of h_c at a particular angular orientation. Temperature differences across the tube wall were successfully measured at only two angular orientations. It is believed that the unsuccessful tests were due to thermocouple bead detachment from the bottom of the channel resulting in significantly lower measured temperatures.

Gas pressures around the tube were measured by rotating a single tube with four 0.063 cm (0.025 in) pressure taps spaced 90° apart.

A channel was also cut in a tube of DS Mar-M 246+Hf and thermocouples placed 0.038 cm (0.015 in) from the surface and covered in an identical manner as that described above for the stainless steel tube. The tube was tested with the channel facing the injector. Surface melting of the Mar-M 246+Hf was observed after one test.

Two tubes of the Ni base superalloy B-1900 were plasma spray coated to two different thicknesses, 0.0076 cm (0.003 in) and 0.024 cm (0.0095 in), with a ZrO_2-8%Y_2O_3 TBC. Thermocouples were attached to the inside wall of these specimens. These coated tubes underwent multiple hot firings with the thermocouple oriented toward the injector.

RESULTS AND DISCUSSION

Representative gas temperatures measured near the test position 2 are shown in Figure 4. Temperatures between the second and third tube (positions A2 and B2) were higher than those between the first and second tube (positions A1 and B1). The variation in gas temperature measurements is indicated in Figure 4a for six measurements made at positions A1 and B1. Two measurements show a temperature difference of approximately 100°C whereas the data from the other four measurements are tightly grouped. Some of this temperature variation is believed due to slightly different positioning of the thermocouples since some temperature nonuniformity in the direction along the cylinder axis was observed. The high temperatures at the beginning of the hot fire are most probably due to the lead in oxygen flow fixed by the valve timing which results in an initially higher O/F ratio and consequent higher temperatures.

A thermal model for the butt-welded thermocouples located at the throat plane was developed to determine the necessary corrections to the measured thermocouple temperatures. A schematic of the thermal model which accounts for recovery, conduction and radiation corrections is shown in Figure 5a. Heat flux to the exposed thermocouple wire was modelled after a cylinder in crossflow. The length of exposed wire varied from 0.18 cm (0.07 in) to 0.36 cm (0.14 in) depending on the wire diameter. Average heat transfer coefficients

for the various wire diameters and fluid properties were taken from Reference 2. As the pressure in the chamber increased at the beginning of the run, the heat transfer coefficient was scaled with the 0.8 power of the normalized chamber pressure ($P/P_{2.07\ MPa}$) to reflect the pressure dependence of the Reynolds number. Thermal conductivities for the Type R and Type B wire were derived from data given in Reference 3 and the emisivity of the wire was taken from Reference 4. The wire was assumed to radiate to room temperature in order to determine the maximum radiation correction. To estimate the actual gas temperature, the predicted thermocouple temperature containing recovery, conduction and radiation corrections was matched to the measured temperatures. The predicted thermocouple temperature is shown as a dashed line in Figure 4. The hot gas temperature input to the model which resulted in the best match of the predicted and measured thermocouple temperature was assumed to be representative of the actual hot gas temperature in the engine at the indicated positions.

The thermal model showed that the three corrections resulted in very little lag in response between the input gas temperature and the predicted thermocouple temperature. The radiation correction amounted to less than 1°C. The effect of recovery and conduction corrections are shown in Figure 5b where after approximately 0.2 seconds into the hot fire, the predicted thermocouple temperature containing corrections is indistinguishable from the input gas temperature.

The measured temperatures are significantly greater than those predicted by equilibrium thermodynamic calculations (Ref. 5) for an O/F=1 and a chamber pressure of 2.07 MPa (300 psi). It is believed that the actual O/F ratio in the engine was greater than that calculated from input flow rates. Because gas temperatures appeared even higher at other cylinder test positions, poor mixing of the gases in the rocket engine chamber can not account for the difference between the calculated and measured gas temperatures.

The measured angular pressure dependence around the cylinder is shown in Figure 6. This pressure dependence is in good agreement with that previously measured for a single cylinder (3.18 cm) and four cylinders (0.953 cm) located at the throat of a square chamber rocket engine (Ref. 6).

Heat transfer coefficients were calculated from temperature differences across the wall of the stainless steel tube (Fig. 7). The value for h_c determined at 90° from the stagnation point and at 180° from the stagnation point was approximately 27.5 kW/m^2°C (4845 Btu/hr/ft^2/°F) and 8.5 kW/m^2°C, respectively. Talmor (Ref. 6) measured and predicted the angular dependence of h_c for tubes at the throat of a square chamber rocket engine. The predicted values were based on the measured presure distribution around the tubes. Talmor's results for the angular dependence of h_c normalized with h_c at the stagnation point are shown in Figure 8. The ratio of h_c at 90° to that at 180° measured in this study (Fig. 8) is in very good agreement with Talmor for the 0.953 cm tubes. Based on this agreement, a value of 27.5 kW/m^2°C was assumed for h_c at the stagnation point for the 0.953 cm tubes and rods used in this study. This value is approximately twice

that predicted for a cylinder in crossflow assuming no turbulence in the approaching gas stream (Ref. 2). This factor of two difference in h_c is a reasonable value for the high levels of turbulence encountered in a rocket engine (Ref. 6).

A thermal model was developed to simulate heat transfer to the tubes and rods, coated and uncoated, in the rocket engine. A schematic of the thermal model is indicated in Figure 9a. A 45° wedge facing the injector was modelled using 22 nodes for a rod and 16 nodes for a tube. Node spacing in the outer layers of the wedge was 0.000254 cm (0.001 in). The heat transfer coefficient for the surface was taken as 27.5 $kW/m^2°C$ in agreement with the results of Talmor (Ref. 6) as discussed above. Temperature dependent material properties for the Mar-M 246+Hf substrate were taken from Reference 7. Temperature dependent properties for the ZrO_2-Y_2O_3 coating were taken from Reference 8. The presence of any metallic bond coat between the ceramic coating and the substrate was assumed to have thermal properties identical to the substrate. For tubes, the inner tube wall was assumed to be insulated. Gas temperatures were those based on the results of the thermocouple models and were essentially those shown as dashed lines in Figures 4a and b. The heat transfer coefficient used for the short H_2 purge at the end of the hot fire was 8.8 $kW/m^2°C$ (1555 $Btu/ft^2/hr/°F$) and that for the N_2 purge was 1.76 $kW/m^2°C$ (311 $Btu/ft^2/hr/°F$). Both coefficients for the H_2 and N_2 purge were approximations based on the chamber pressures and fluid properties (Ref. 2).

Measured and predicted temperatures at 0.038 cm (0.015 in) below the surface of a bare Mar-M 246 tube are shown in Figure 9b. Although the measured gas temperature exceeds the predicted temperature by 50°C at the maximum temperature, the agreement between the predicted and measured temperatures for most of the heatup and cooldown period is very good. The 50°C difference is within the uncertainty in gas temperatures along the length of the test specimen.

Measured and predicted temperatures on the inner wall of the B-1900 superalloy with a 0.0076 cm (0.003 in) and 0.024 cm (0.0095 in) TBC coating are shown in Figure 9c. It is apparent that the thermal model significantly underpredicts the measured temperatures. Two reasons could account for this large discrepancy. If the hot hydrogen-rich gas penetrates the porous ZrO_2 layer, the thermal conductivity used for the ZrO_2 may be innapropriate. Similarly, the surface roughness of the plasma-sprayed coating may significantly increase the turbulence around the tube increasing the heat transfer coefficient above that measured with the smooth stainless steel tube. The effect of surface roughness is being investigated in a series of verification tests. Although the temperature reduction due to the TBC is not as great as predicted, it is significant that the 0.0076 cm (0.003 in) TBC reduced the temperature at the inner wall by approximately 100°C and the 0.024 cm (0.0095 in) TBC reduced the inner wall temperature by more than 300°C in comparison to the predicted inner wall temperatures for an uncoated tube.

TBC durability in the rocket engine was greater for rods than for

tubes (Ref. 1). Temperature profiles through a coated tube and rod were predicted to examine the cause of this difference. A constant gas temperature of 1371°C (2500°F) for a 1 second exposure was used to simplify this comparison. The temperature profile through a 0.015 cm (0.006 in) ZrO_2 coating and substrate is shown in Figure 10a and the time dependence of the temperature on the surface of the coating and at the coating-metal interface is shown in Figure 10b. It is apparent that the metal temperature at the surface of the tube is more than 55°C greater than the metal temperature of the rod. Coating degradation is usually linked with thermally activated processes which would suggest a shorter coating life for the tubes which exhibit significantly increased substrate temperatures.

A thermal model of the leading edge of the SSME HPFTP blade was constructed to evaluate the potential of TBC's to reduce the blade metal temperature during the thermal transient which occurs on engine startup. A schematic of the thermal model is shown in Figure 11. The gas temperature for the thermal transient on startup was taken from Reference 9. The actual heat transfer coefficient on the HPFTP blade varies as the pressure in the turbine increases. Reference 10 indicates that the pressure during the thermal transient is a small fraction of that at steady state. A heat transfer coefficient of 7.65 $kW/m^2/°C$ (1350 $Btu/ft^2/hr/°F$) was chosen which produced a maximum surface metal temperature of 1000°C, equivalent to that predicted in Reference 9 for the leading edge near the tip for the identical temperature transient. Figure 12 shows the temperature profile and the predicted surface temperature for an uncoated surface. Also shown are predicted surface metal temperatures below 0.0064 cm (0.0025 in) and 0.017 cm (0.0065 in) thick ZrO_2 TBC's. The 0.0064 cm (0.0025 in) coating reduces the surface metal temperature at the end of the thermal transient by 250°C while the 0.017 cm (0.0065 in) coating reduces the temperature by 450°C. Based on the previous experimental results, these temperature decreases may not be totally realized, but the results indicate that TBC's can be used to significantly reduce metal temperatures.

The initial heat flux to the blade can be estimated as $h_c \Delta T$ where ΔT is the maximum temperature during the thermal transient minus the initial temperature. Assuming that the heat transfer coefficient used in modelling the leading edge in this study is indicative of that in the HPFTP during the thermal transient, and taking the value of ΔT for the HPFTP as approximately 1800°C (Ref. 9), results in a maximum heat flux of 13800 kW/m^2. The value of ΔT for test position 2 in the rocket engine at LeRC is 1280°C which, for h_c=27.5 $kW/m^2°C$ used above produces a maximum heat flux of 35200 kW/m^2 for the conditions used in this test. It is significant to note that the maximum heat flux in the rocket engine at LeRC appears somewhat greater than that in the HPFTP during the initial thermal transient based on the above assumptions. However, the heat flux during steady state operation of the HPFTP is significantly greater.

SUMMARY AND CONCLUSIONS

Gas temperatures and pressures were measured around the second test position in the H_2/O_2 rocket engine at NASA Lewis. Measured gas temperatures generally varied from 1210°C to 1390°C. Measured pressures were in good agreement with other studies for throat tubes in a square chamber rocket engine. Heat transfer coefficients were measured at 90° and 180° from the stagnation point and resulted in values of 27.5 $kW/m^2°C$ and 8.5 $kW/m^2°C$, respectively. A thermal model was developed to predict temperatures in bare and coated tubes and rods. Agreement between measured and predicted temperatures below the surface of a bare Mar-M 246 tube was very good for most of the heatup and cooldown period. Predicted temperatures were significantly below measured temperatures for the coated tubes. A thermal model to simulate heat transfer to the leading edge of an HPFTP blade was developed and showed that TBC's can significantly dampen the thermal transient which occurs in the HPFTP during startup of the SSME.

REFERENCES

1. W.J. Brindley and J.A. Nesbitt, "Durability of Thermal Barrier Coatings in a High Heat Flux Environment", 1988 Conference on Advanced Earth-To-Orbit Propulsion Technology, May 10-12, 1988, Huntsville, Alabama.
2. F. Kreith, Principles of Heat Transfer, 2nd Edition, International Textbook Co. Scranton, PA, 1965.
3. Thermophysical Properties of Matter, Vol. 1., Thermal Conductivity, Y.S. Touloukian, R.W. Powell, C.Y. Ho and P.G. Klemens, eds., Plenum Press, New York, 1970.
4. Thermophysical Properties of Matter, Vol. 7., Thermal Radiative Properties, Y.S. Touloukian, R.W. Powell, C.Y. Ho and P.G. Klemens, eds., Plenum Press, New York, 1970.
5. S. Gordon and B.J. McBride, "Computer Program for Calculation of Complex Chemical Equilibrium Compositions, Rocket Performance, Incident and Reflected Shocks, and Chapman-Jouguet Detonations", NASA SP-273, March 1976.
6. E. Talmor, "Heat Transfer to Small Diameter Throat Tubes", 56th National Meeting of the American Institute of Chemical Engineers, San Francisco, CA, May 16-19, 1965, AIChE Preprint.
7. W.T. Chandler, "Materials for Advanced Rocket Engine Turbopump Blades", NASA CR-174729, November, 1983.
8. T.E. Strangman, J. Neumann and A. Liu, "Thermal Barrier Coating Life-Prediction Model Development", NASA CR-179648, October 1987.
9. A. Abdul-Aziz, M.T. Tong and A. Kaufman, "Thermal Finite-Element Analysis of Space Shuttle Main Engine Turbine Blade", NASA TM-100117, October 1987.
10. J.F. Newell, "Composite Loads Spectra for Select Space Propulsion Structural Components", in Structural Integrity and Durability of Reusable Space Propulsion Systems, NASA CP 2381, p. 67, 1985.

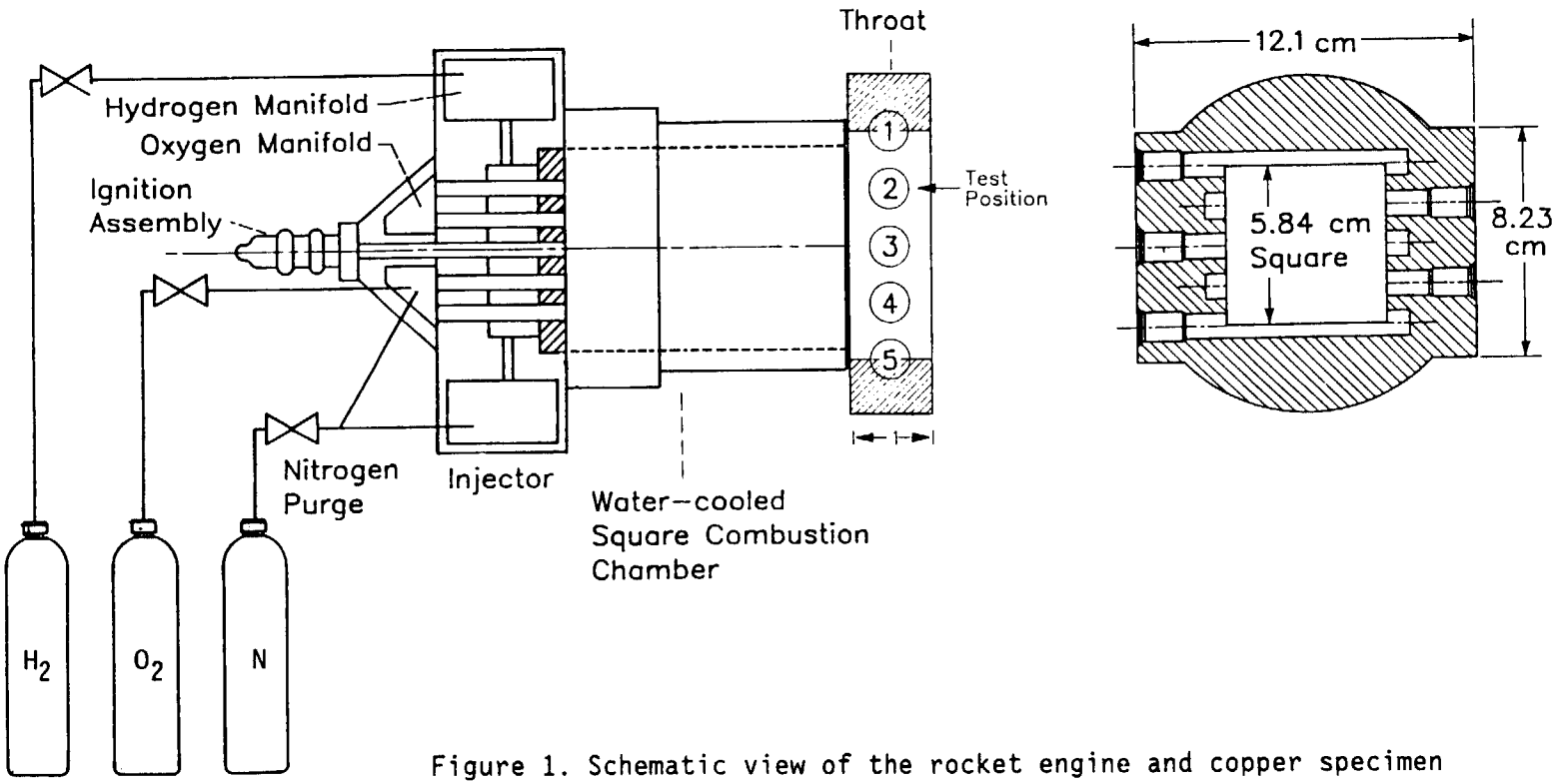

Figure 1. Schematic view of the rocket engine and copper specimen holder

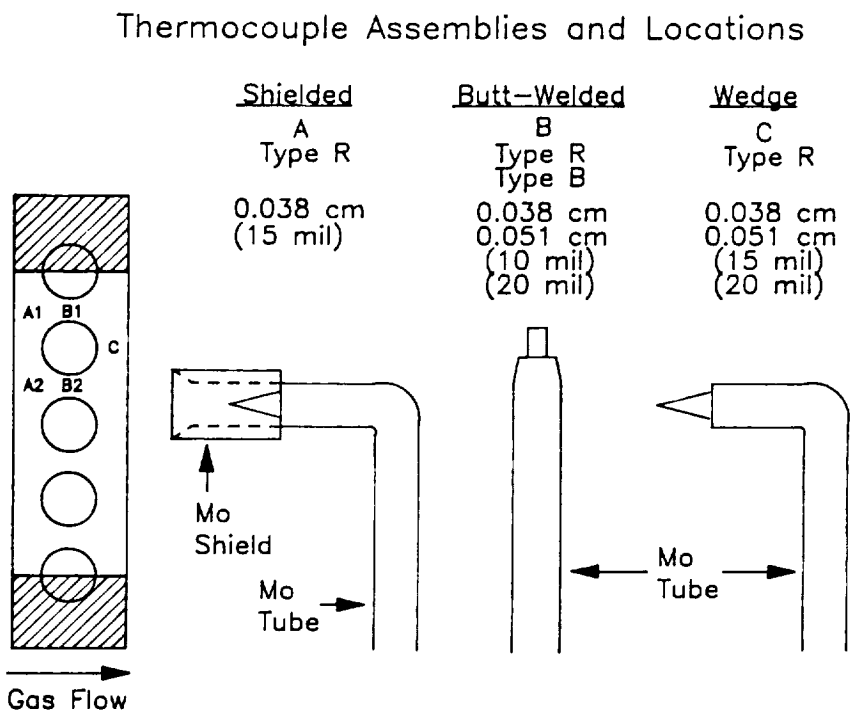

Figure 2. Schematic view of the thermocouple probe assemblies used to measure gas temperatures

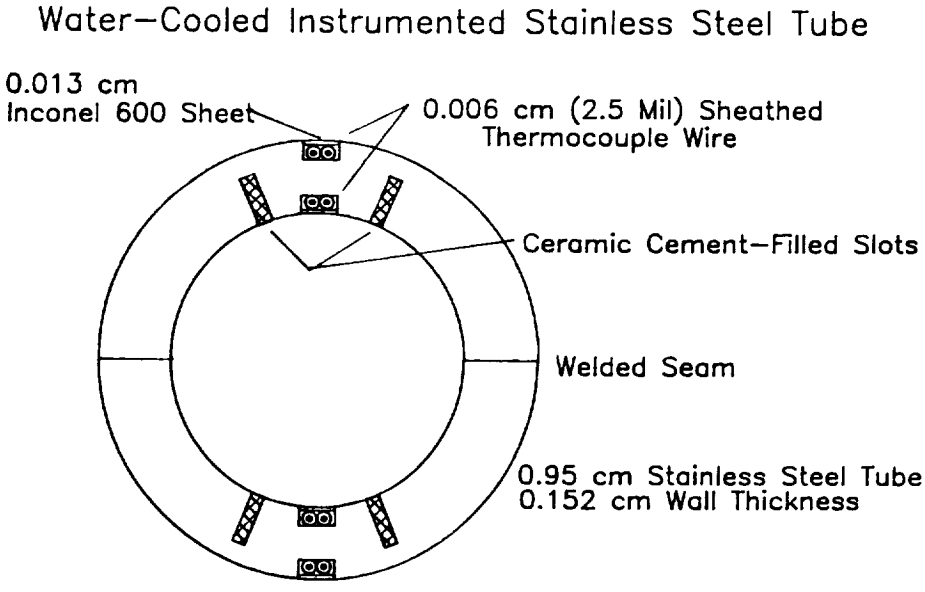

Figure 3. Schematic cross section of the instrumented stainless steel tube used for measuring heat transfer coefficients

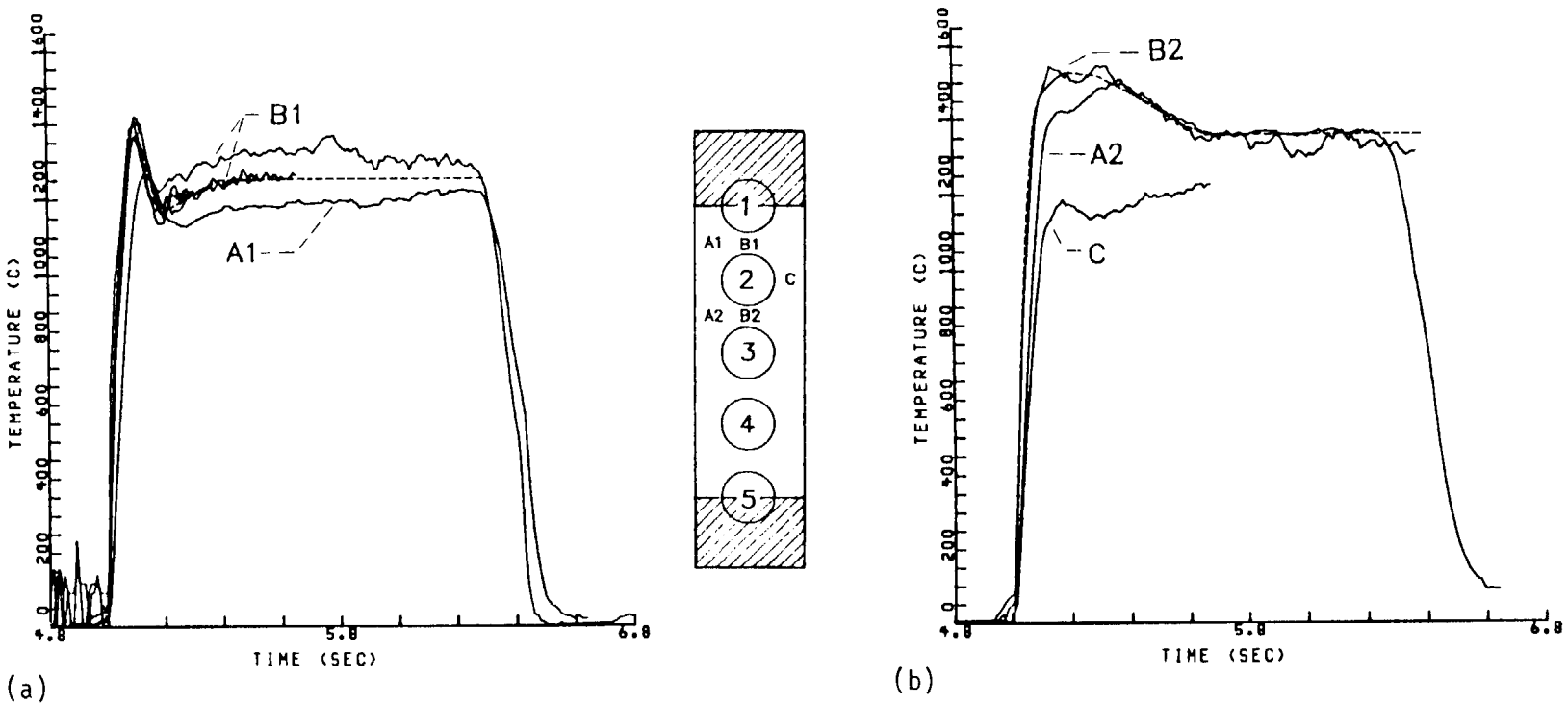

Figure 4. Gas temperatures measured between test positions (a) 1 and 2, (b) 2 and 3

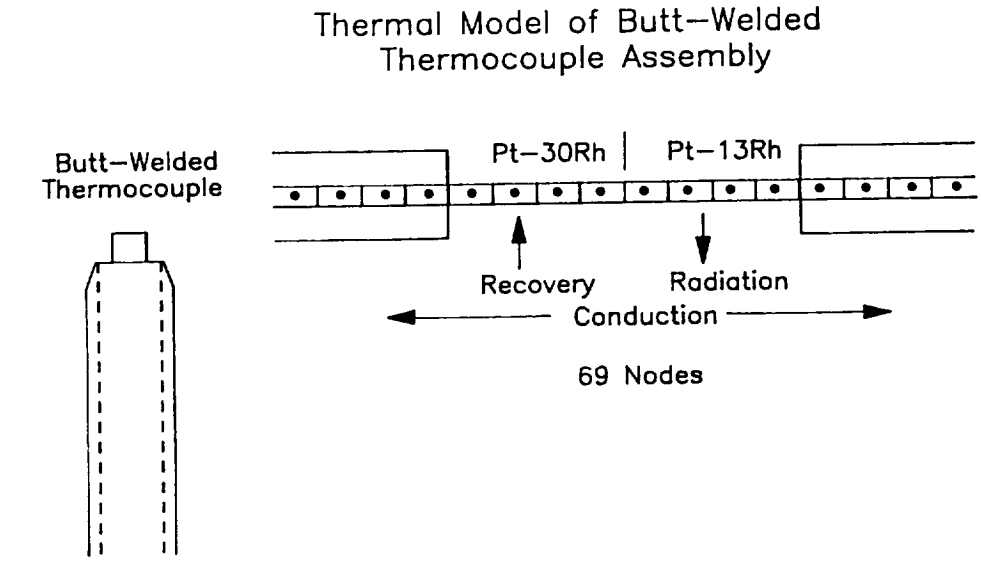

(a)

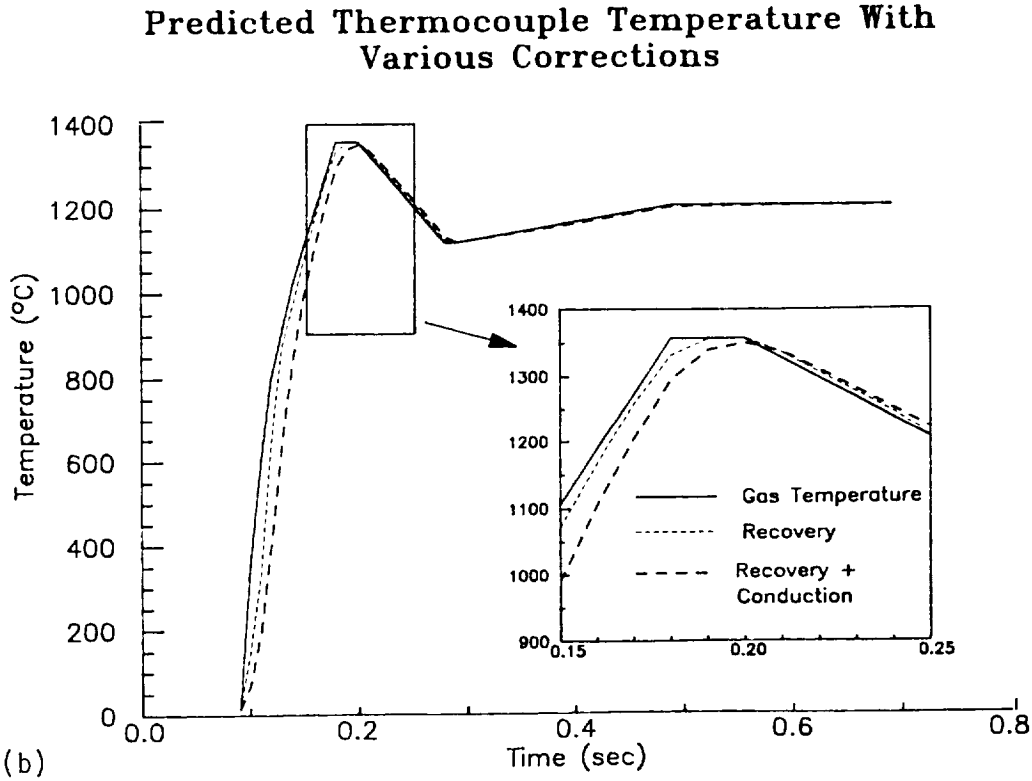

(b)

Figure 5. Thermal analysis of the butt-welded thermocouples, (a) thermal model of thermocouple assembly, (b) predicted thermocouple temperatures with various corrections

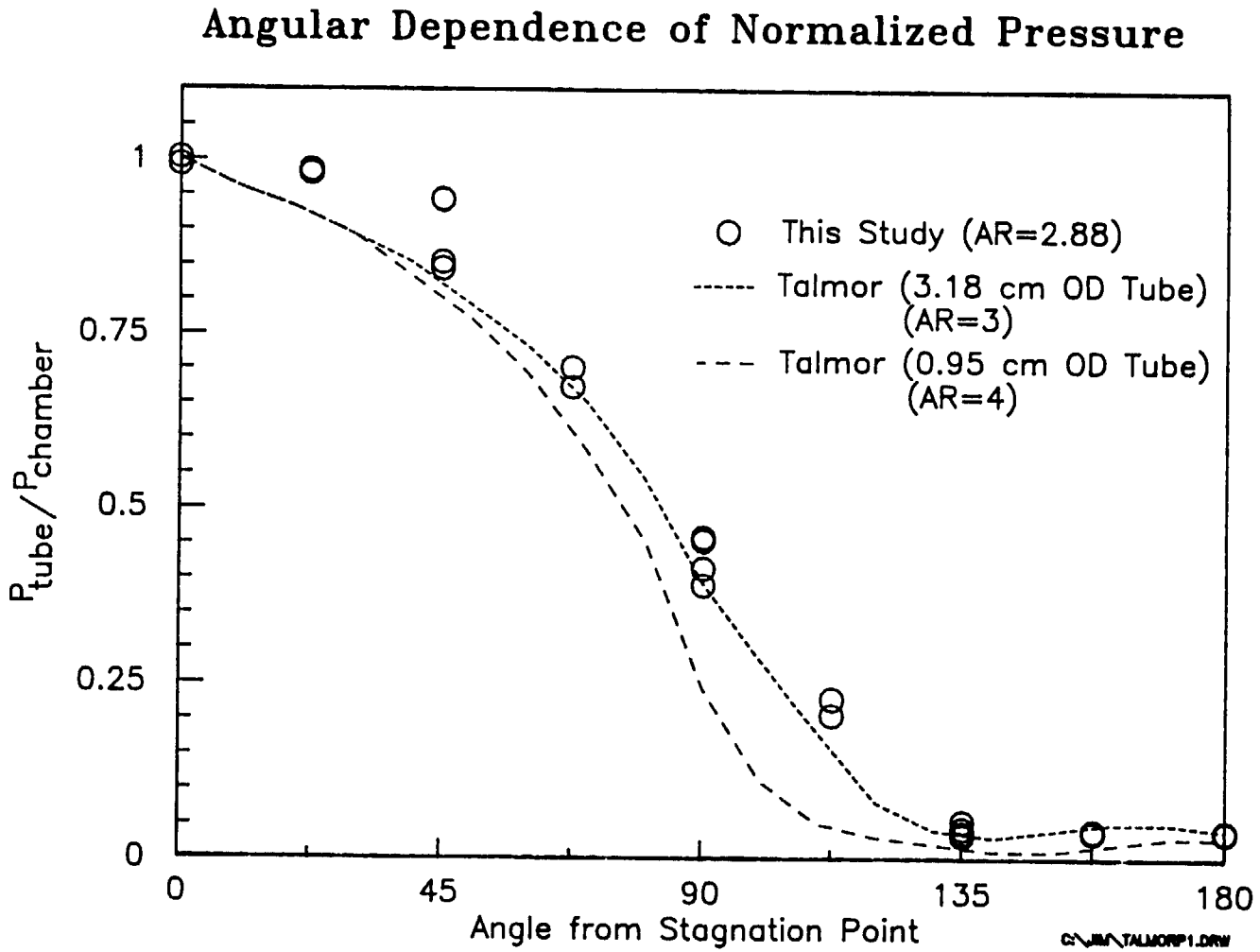

Figure 6. Measured and reported (Ref. 6) angular pressure distributions (AR=area reduction at throat)

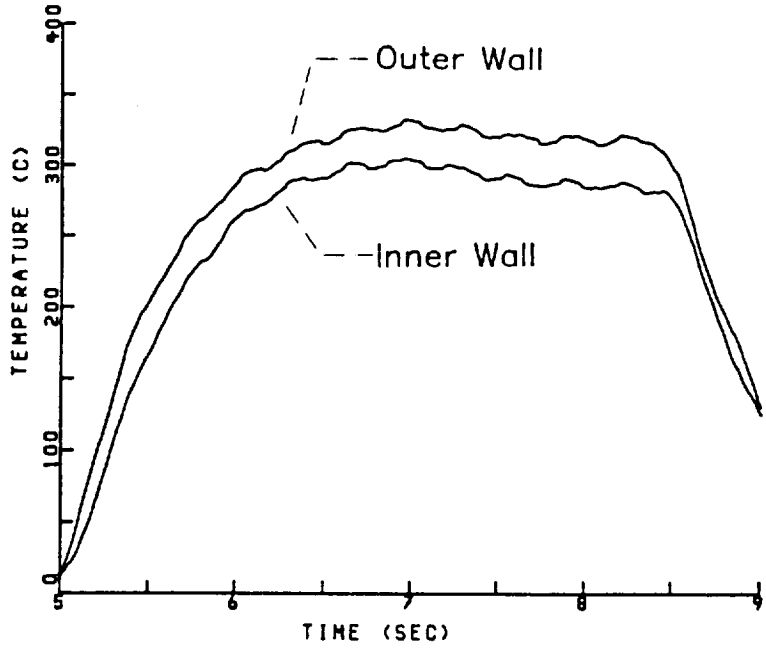

Figure 7. Wall temperatures in water-cooled stainless steel tube used for determining heat transfer coefficients

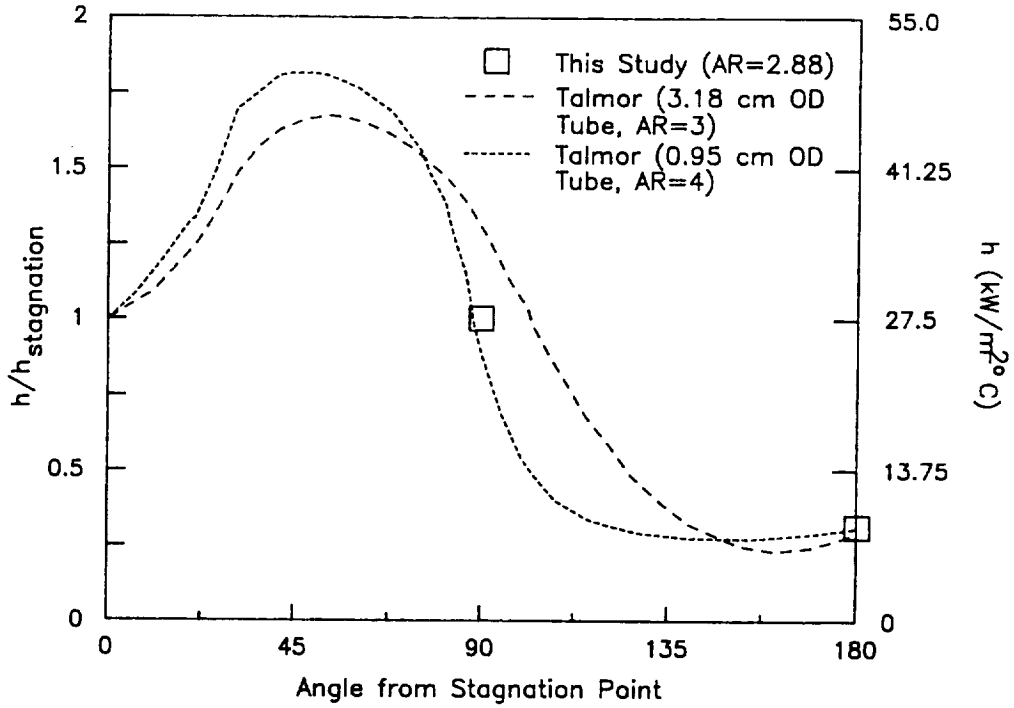

Figure 8. Reported angular heat transfer distributions (Ref. 6) and measured heat transfer coefficients

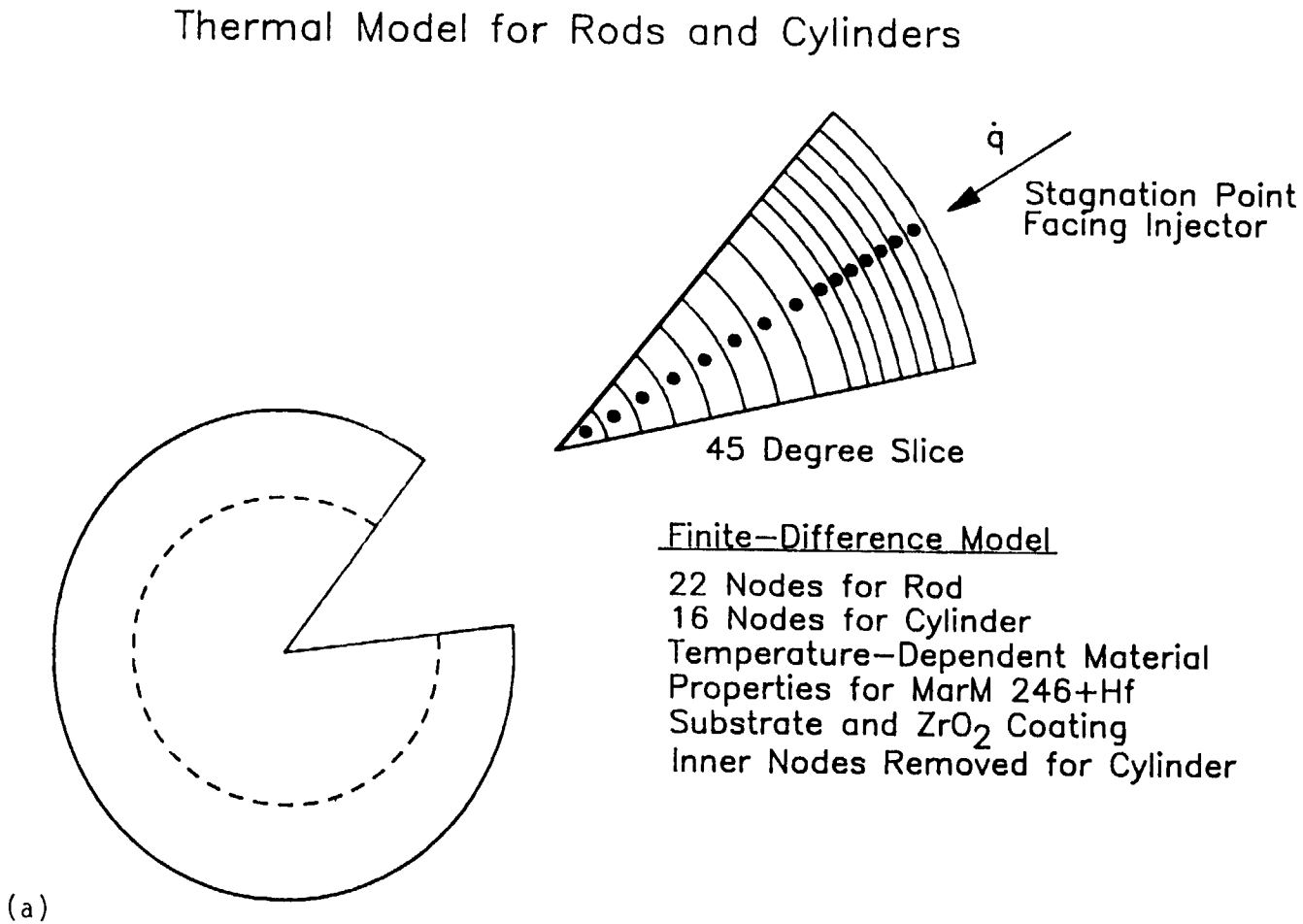

Figure 9. Thermal analysis of rods and tubes (a) thermal model

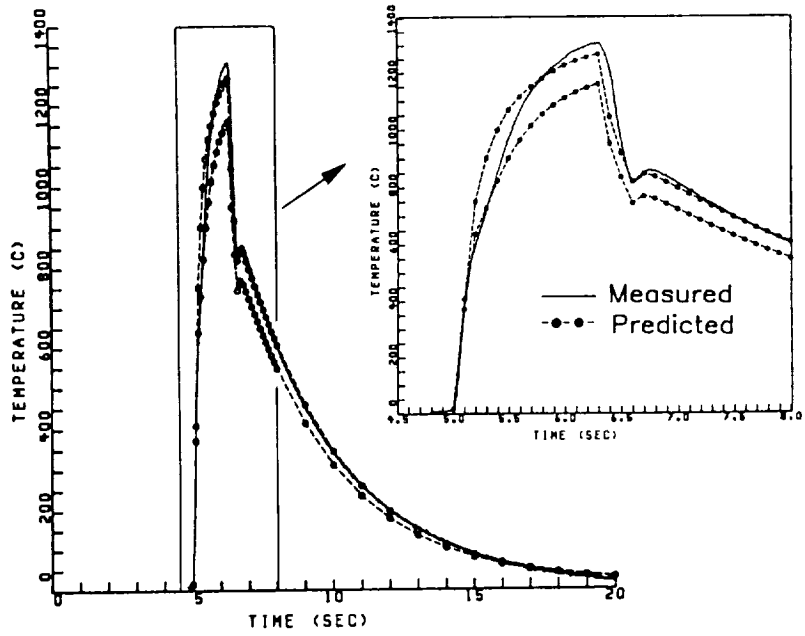

(b)

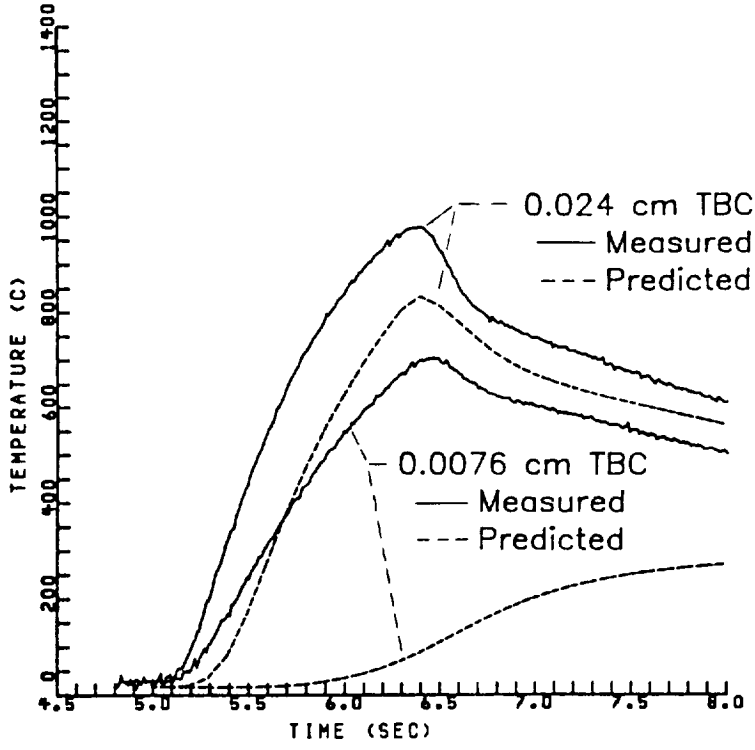

(c)

Figure 9. Thermal analysis of rods and tubes (continued) (b) measured and predicted temperatures near the surface of the Mar-M 246+Hf tube, (c) measured and predicted temperatures on the inside wall for two TBC coated tubes of B-1900

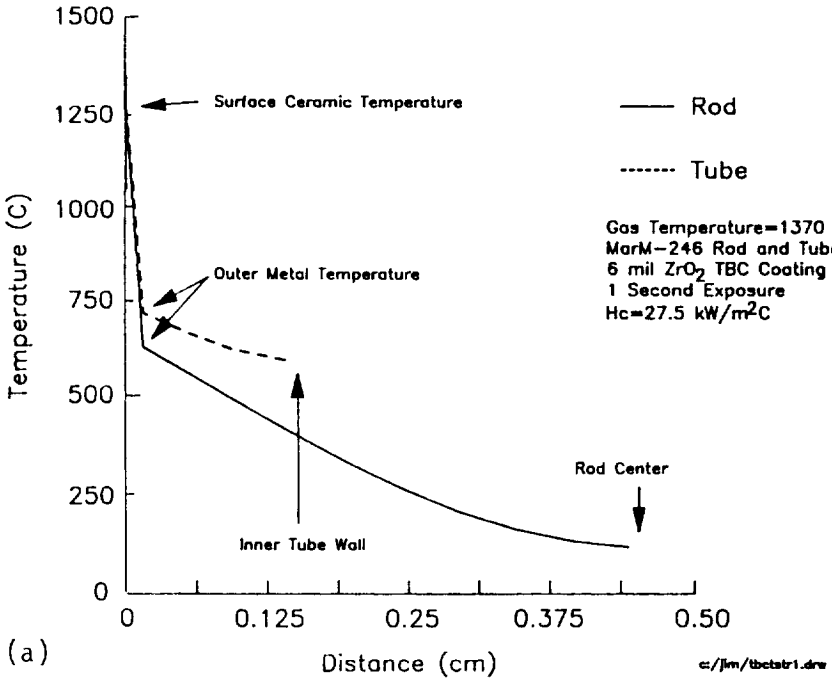

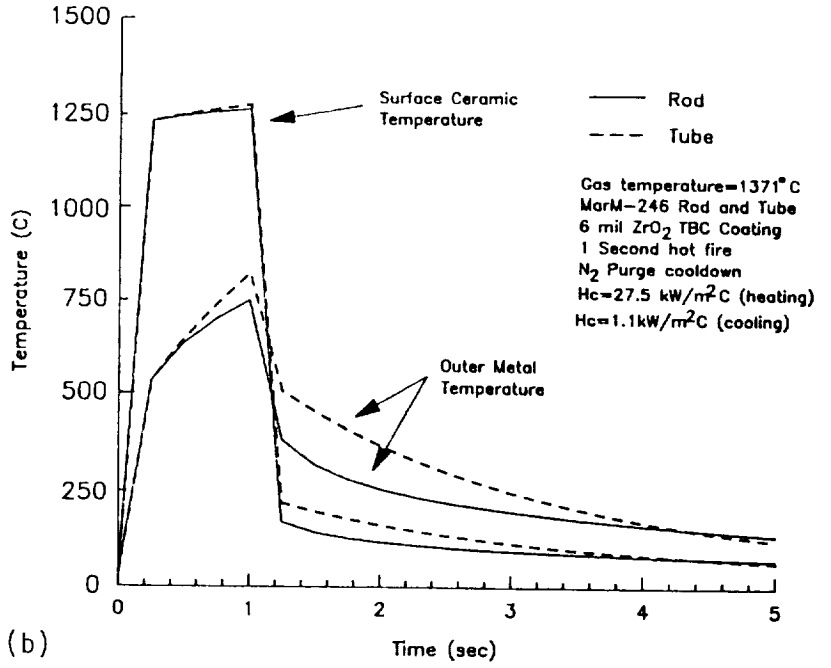

Figure 10. Predicted Temperatures for tubes and rods (a) temperature profile through coating and substrate, (b) temperature on coating surface and at coating-metal interface

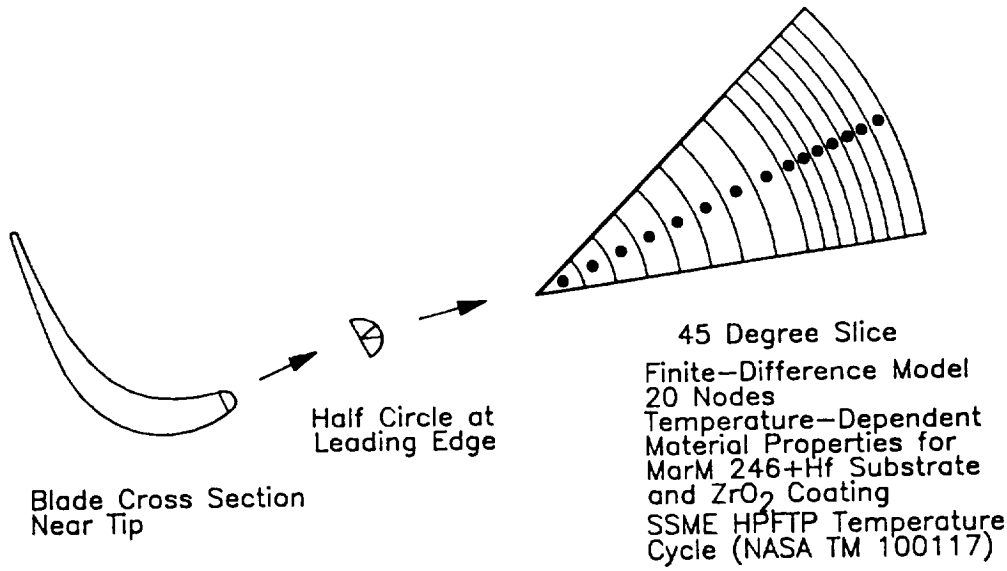

Figure 11. Thermal model for leading edge of HPFTP blade

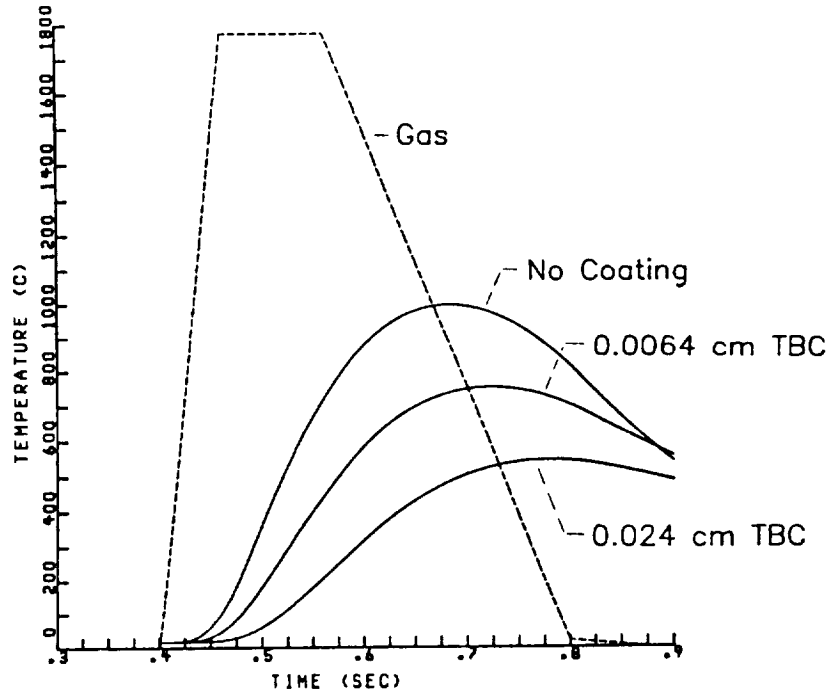

Figure 12. Predicted temperatures for HPFTP blade metal surface without coating and two TBC coating thicknesses